Effects of an external magnetic field on the hyperfine parameters in RE_2O_3 (RE = Gd, Er) nanoparticles measured by perturbed angular correlation spectroscopy

Cite as: AIP Advances **10**, 015039 (2020); https://doi.org/10.1063/1.5130401
Submitted: 03 October 2019 . Accepted: 27 December 2019 . Published Online: 17 January 2020

E. L. Correa, B. Bosch-Santos, R. N. Saxena, G. A. Cabrera-Pasca, and A. W. Carbonari

Effects of an external magnetic field on the hyperfine parameters in RE_2O_3 (RE = Gd, Er) nanoparticles measured by perturbed angular correlation spectroscopy

Cite as: AIP Advances 10, 015039 (2020); doi: 10.1063/1.5130401
Presented: 6 November 2019 • Submitted: 3 October 2019 •
Accepted: 27 December 2019 • Published Online: 17 January 2020

E. L. Correa,[1,a)] B. Bosch-Santos,[1] R. N. Saxena,[1] G. A. Cabrera-Pasca,[2] and A. W. Carbonari[1]

AFFILIATIONS

[1]Nuclear and Energy Research Institute, 05508-000 São Paulo, SP, Brazil
[2]Federal University of Para, 68440-000 Abaetetuba, PA, Brazil

Note: This paper was presented at the 64th Annual Conference on Magnetism and Magnetic Materials.
[a)]Nuclear and Energy Research Institute, 05508-000 São Paulo, SP, Brazil; **Electronic mail:** eduardo.correa@usp.br

ABSTRACT

In order to understand the interaction mechanisms in RE_2O_3 (RE=Gd, Er) nanoparticles (NPs), Perturbed Angular Correlation (PAC) spectroscopy, a local technique, plus external magnetic field, was used to elucidate local interactions and possible mapping of the different contribution in these compounds. NPs were synthesized by thermal decomposition and characterized by transmission electron microscopy and X-ray diffraction. PAC measurements were performed using $^{111}In(^{111}Cd)$ as probe nuclei, with and without the application of an external magnetic field (EMF) of 0.5 T in different temperatures (50 K, 100 K, 200 K, 300 K). Results show that the hyperfine magnetic field is almost zero when the probe is located at the symmetric site, and ~4 T and ~5 T for Gd_2O_3 and Er_2O_3, respectively, when the probe occupies the asymmetric field.

I. INTRODUCTION

The rare-earth (RE) oxides present three different structures depending on the RE ionic radii: hexagonal (A-type), monoclinic (B-type) or cubic (C-type).[1] In the latter, RE ions occupy two non-equivalent cation sites: asymmetric 24d sites and symmetric 8b sites. Gd_2O_3 and Er_2O_3 crystallize in this structure and have a paramagnetic behavior, although Er_2O_3 also orders antiferromagnetically below 4 K.[2,3] The magnetic properties of these compounds, especially in the nanoparticle (NP) form, present potential for many applications, both technological and medical.[4–6] Thus, to understand the mechanism of these properties is of great significance. Several works have been done in order to determine magnetic properties in NPs.[7–10] It is well known that NPs, due small size, present magnetic characteristics that can be attributed to: (a) core magnetic contribution, due to crystalline structure (point symmetry of magnetic atom) and exchange interactions and (b) surface contributions, due to canted spins or spin-glass-like behavior of the surface spins.

Therefore, an investigation of the localized magnetic moment behavior on Gd and Er sites in Gd_2O_3 and Er_2O_3 NP, within an atomic resolution, under the influence of an external magnetic field (EMF), is very necessary to understand the magnetic behavior of these compounds and how this information is passed throughout the structure. In this paper, Perturbed Angular Correlation (PAC) spectroscopy using $^{111}In(^{111}Cd)$ as probe nuclei, a local technique, plus EMF with magnitude of 0.5 T, was used to investigate local interactions in Gd_2O_3 and Er_2O_3 NPs. PAC measurements with EMF have already been made and results have shown that a hyperfine magnetic field (B_{hf}) is induced to the sample.[11] The objective here is to determine which kind of interaction is more likely to happen in these compounds.

II. MATERIALS AND METHODS

A. Synthesis and characterization of rare-earth nanoparticles

Rare-earth nanoparticles (RENP) were synthesized by a modified thermal decomposition.[3] Around 10 μL of a radioactive $^{111}InCl_3$ solution was added during sample preparation for PAC measurements. After the almost complete ^{111}In decay samples were structurally characterized by X-ray diffraction (XRD) using a Philips X'Pert diffractometer and analyzed by Rietveld method, and NPs shape, size and size distribution were determined by transmission electron microscopy (TEM), using a Joel JEM-2100 microscope.

B. PAC spectroscopy measurements

For PAC measurements ^{111}Cd, produced after the decay of ^{111}In, was used as probe nuclei. The spectrometer consists of four BaF_2 detectors associated with a slow-fast electronic setup used to measure delayed γ-γ coincidences. In this technique two gamma rays in a cascade emitted as a result of the probe nuclei decay from excited levels are detected. Angular correlation of gamma radiation is perturbed by the interaction between intermediate nuclear state moment and extra nuclear fields. The coincidence spectra data is processed to obtain the spin rotation function $R(t)=A_{22}G_{22}(t)$, where A_{22} is the anisotropy factor and $G_{22}(t)$ is the perturbation function. The measurement allows the determination of the nuclear quadrupole frequency $\nu_Q = eQV_{zz}/h$, asymmetry parameter $\eta = (V_{xx} - V_{yy})/V_{zz}$ and the Larmor frequency $\omega_L = \hbar B_{hf}/g\mu_N$, where μ_N is nuclear magneton for magnetic dipole interactions and Q and g are the electric quadrupole moment and the g-factor of the probe nuclei, respectively. V_{kk} (k=x,y,z) denote the main components of the electric field gradient (efg) tensor. The perturbation function allows the determination of the efg and B_{hf}. More information about PAC spectroscopy can be found elsewhere.[12,13] In this study samples were placed inside a closed cycle refrigerator (CCR) together with four magnets (two below and two above the sample). The applied field is 0.5 T, and temperatures used were 50 K, 100 K, 200 K and 300 K.

III. RESULTS

A. XRD and TEM

TEM images, together with the respective histogram and XRD patterns, show NPs with average size of 14.9 nm and 15 nm for Gd_2O_3 (FIG. 1) and Er_2O_3 (FIG. 2), respectively, with a narrow size distribution for both compounds. X-ray results have shown that both samples have crystallized in the cubic C-type structure with $Ia - 3$ space group (bixbyite). Lattice parameters are a=b=c=10.805(1) Å and a=b=c=10.553(1) Å for Gd_2O_3 and Er_2O_3, respectively, which are in accordance with previous studies.[14,15] The unit cell of a bixbyite structure contains 48 oxygen and 32 metal atoms sitting on two non-equivalent sites: site 8b (1/4 1/4 1/4) and 24d (x 0 1/4), where x=0.0307(4) for Gd_2O_3 and x=−0.0325(5) for Er_2O_3, Wyckoff positions, where the first site is occupied by 8 metal atoms with D_{3d} symmetry and the second is occupied by 24 metal atoms with C_2 symmetry.[16] The O^{2-} are on the 48e (x y z) position, where x=0.3910(5), y=0.0153(5) and z=0.3779(4) for Gd_2O_3 and x=0.3910(4), y=0.1521(5) and z=0.3786(4) for Er_2O_3.

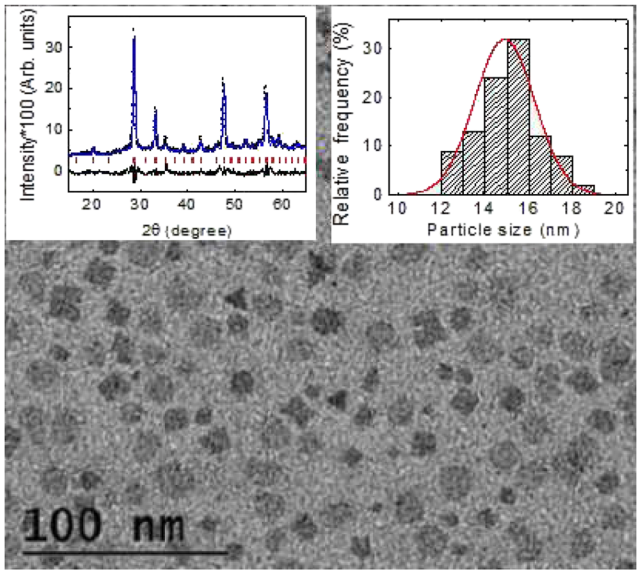

FIG. 1. Transmission electron microscopy image of Gd_2O_3 sample. The insets show X-ray diffraction patterns (left) and the histogram with nanoparticles size distribution (right).

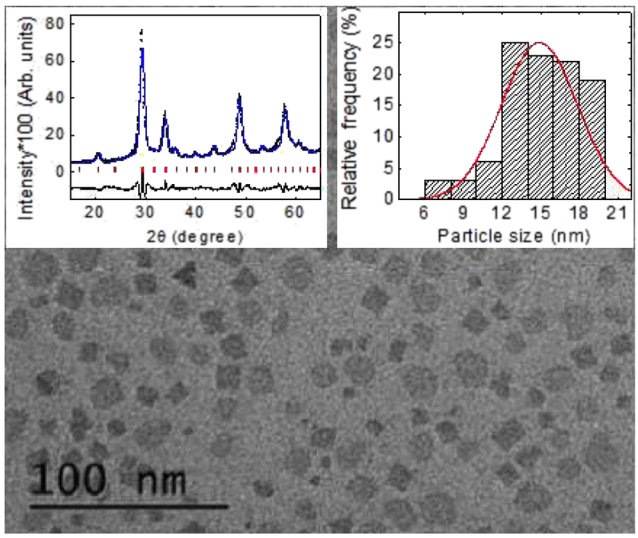

FIG. 2. Transmission electron microscopy image of Er_2O_3 sample. The insets show X-ray diffraction patterns (left) and the histogram with nanoparticles size distribution (right).

B. PAC measurements

PAC spectra obtained without the EMF were fitted with a model considering pure electrical quadrupole interactions (EQI) at ^{111}Cd probes occupying three different sites: symmetric 8b (site 1), asymmetric 24d (site 2), and a third site assigned to probes located at the surface of the NPs (site 3).[3] To make the results comparison clearer, the fractions were normalized for sites 1 and 2. Furthermore, only the effect of the EMF on these sites will be discussed here, since the hyperfine magnetic field present on the NPs' surface is highly distributed and not measurable. According to Zacate[13] the effect of a magnetic field at the probe nuclei is the same, for the same field intensity and the same probe, regardless of the field source, i.e., if the EMF is produced by a magnet or, in the case of ferromagnetic and antiferromagnetic materials, by the own sample. Thus, for PAC spectra obtained with the application of the EMF a model combining EQI plus magnetic dipole interaction was used.[17,18] PAC results for Gd_2O_3 (FIG. 3) and Er_2O_3 (FIG. 4) show a damping of the R(t) amplitude when the EMF is applied.

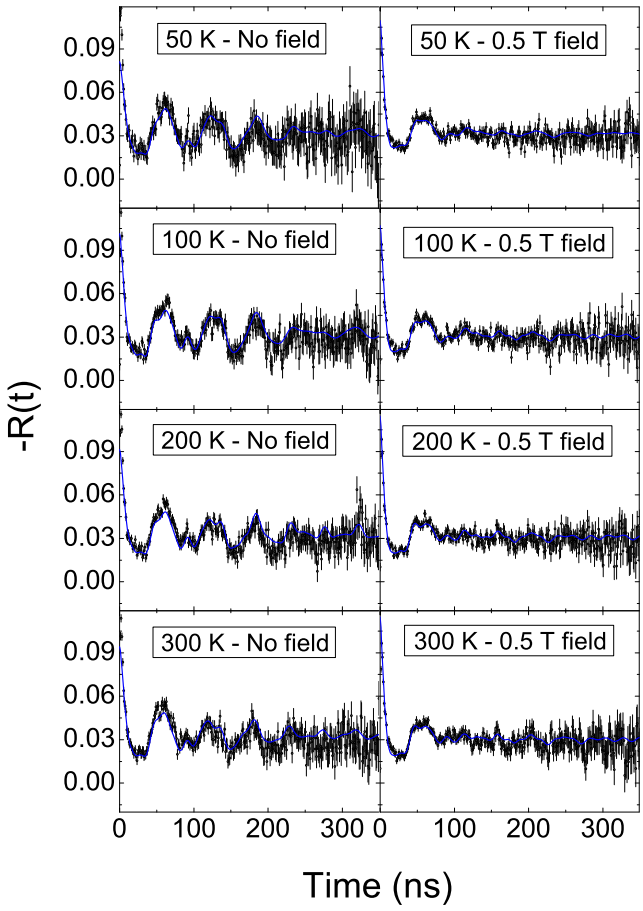

FIG. 3. Spin rotation function (-R(t)) in different temperatures for Gd_2O_3 samples with and without an external magnetic field of 0.5 T.

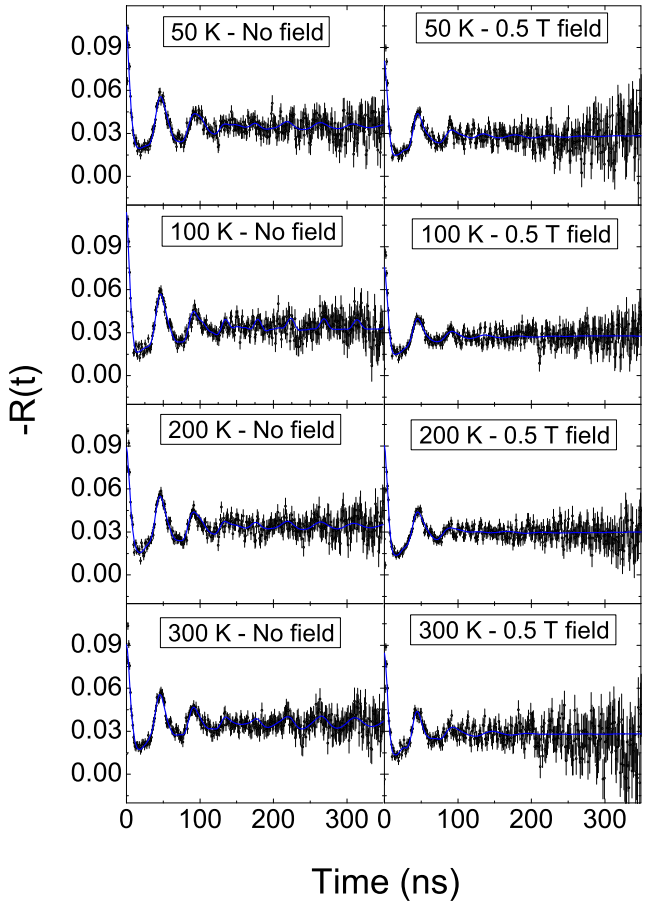

FIG. 4. Spin rotation function (-R(t)) in different temperatures for Er_2O_3 samples with and without an external magnetic field of 0.5 T.

The hyperfine parameters for Gd_2O_3 show that, at room temperature, about 25% of the probe nuclei occupy the symmetric site, characterized by a quadrupole frequency ν_Q=145 MHz, asymmetry parameter η=0.11 and frequency distribution parameter δ=1.7%. Under same conditions about 75% of the probe nucleus occupy the asymmetric sites, characterized by ν_Q=63 MHz, η=1 and δ=8.3%. These parameters do not change greatly in the temperature range studied (FIG. 5). These values are in accordance with previous studies of PAC measurements in Gd_2O_3 bulk.[19] Results obtained with EMF show that about 18% of the probe nucleus occupy the site that presents ν_Q=147 MHz, η=0, δ=1.4%. The total hyperfine magnetic field (B_{hf}(total)) presented is a sum of B_{hf} in the sample and the EMF intensity, thus, B_{hf}(total)=B_{hf}(sample)+B(EMF). For this site, B_{hf} ~0 T, which means that the probe nuclei located in this site is very little affected by the EMF. On the other hand, about 82% of the probe nucleus occupy the site characterized by ν_Q=68 MHz, η=1 and δ=17%. In this case, B_{hf} ~4 T, which means that ^{111}Cd located at this site is affected by the EMF. These parameters do not change significantly with temperature (FIG. 5).

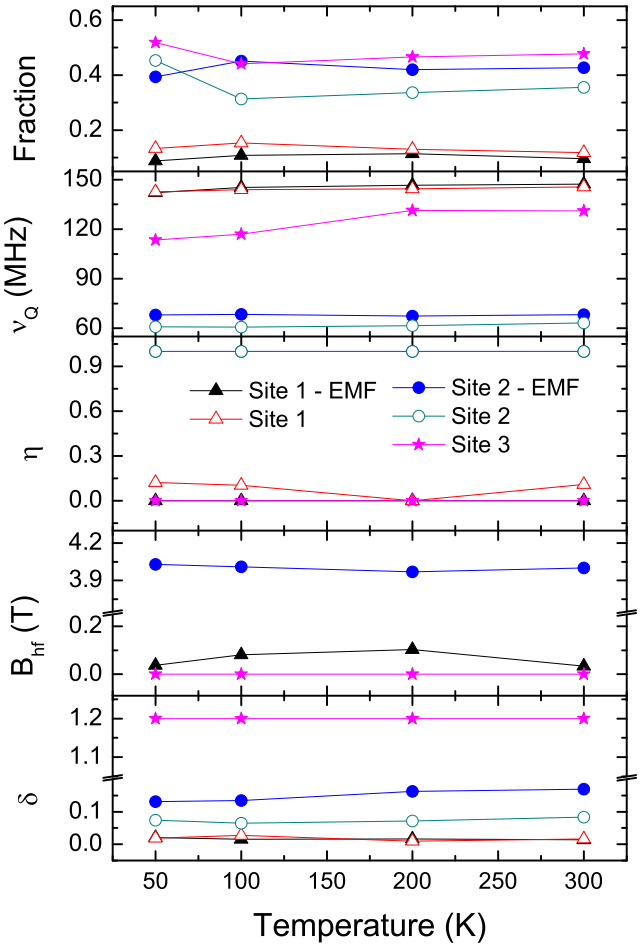

FIG. 5. Hyperfine parameters for Gd_2O_3 measured with and without application of an external magnetic field (EMF) for sites 1 (symmetric), 2 (asymmetric) and 3 (surface). The solid curves are only to guide the eyes.

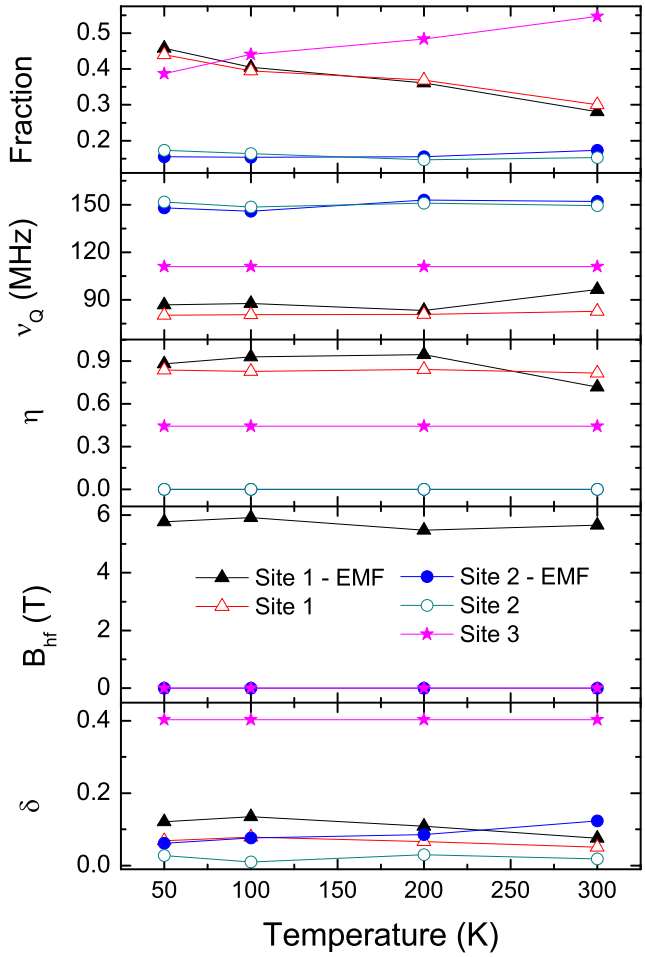

FIG. 6. Hyperfine parameters for Er_2O_3 measured with and without application of an external magnetic field (EMF) for sites 1 (symmetric), 2 (asymmetric) and 3 (surface). The solid curves are only to guide the eyes.

One can note that hyperfine parameters do not change greatly with the application of the EMF. However, the value of B_{hf} at asymmetric sites is much higher than at symmetric sites, and constant for different temperatures. Results for Er_2O_3 show that 21% of the probe nucleus occupy the symmetric sites, presenting ν_Q=149 MHz, η=0 and δ=1.8%, and 79% occupy the asymmetric sites, with ν_Q=83 MHz, η=0.82 and δ=5%. No significant change in the hyperfine parameters with temperature has been observed (FIG. 6). These values are in accordance with those presented in the literature for Er_2O_3.[16] Results obtained with the EMF show around 38% of the probes present ν_Q=151 MHz, η=0 and δ=12.4%, and 62% present ν_Q=97 MHz, η=0.72 and δ=7.5%. B_{hf} ~0 T for the symmetric site and ~5 T for the asymmetric site (FIG. 6). Hyperfine parameters do not change greatly in the temperature range studied. As well as Gd_2O_3 samples, hyperfine parameters for Er_2O_3 do not present a significant change with the application of the EMF, and B_{hf} at the asymmetric site is much higher than that of the symmetric site (~0 T).

IV. DISCUSSIONS

The application of the EMF affected these systems in two ways: first, all spectra show a damping in the amplitude (FIG. 3 and 4), which is characteristic of uncompensated spin and/or distortion in the crystalline structure distributions due to uncompensated bonds between RE-O; second, the asymmetric site presented B_{hf} ~4 T for Gd_2O_3 and B_{hf} ~5 T for Er_2O_3, and the symmetric site presented B_{hf} ~0 T for both samples. The probe located at the asymmetric site is surrounded by four symmetric sites and eight asymmetric sites (FIG. 7–a). However, the probe located at the symmetric site is surrounded by 12 asymmetric sites (FIG. 7–b). Detailed symmetry of each site is shown in FIG. 7–c.

Results straightforwardly indicated that the exchange coupling between the rare-earth atoms in both Gd_2O_3 and Er_2O_3 oxides is antiferromagnetic because B_{hf} vanishes for probe nuclei at RE1 sites due to the symmetry whereas it is non-zero for probes at RE2 sites (asymmetric sites). In addition, in oxides the coupling is mediated

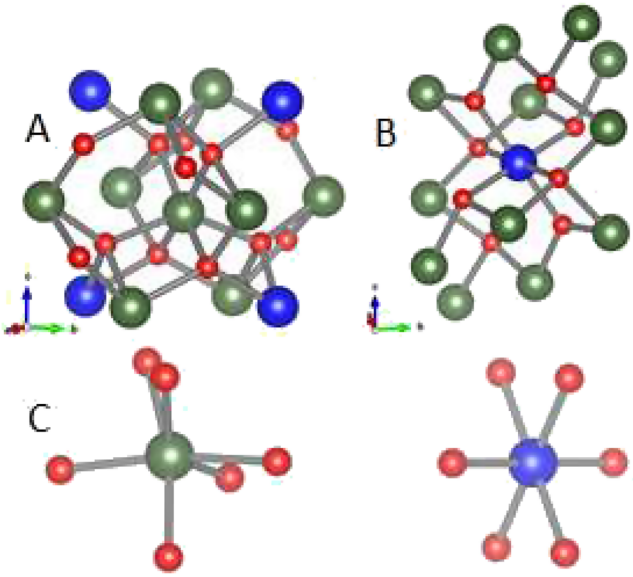

FIG. 7. Central atoms and the respective first neighbors in the (a) asymmetric and (b) symmetric sites in a bixbyite structure. (c) Detail of the asymmetric (green sphere) and symmetric (blue sphere) sites. Red spheres are oxygen atoms.

by superexchange interactions, which are usually antiferromagnetic according to the Goodenough-Kanamori rules.[20,21] In the superexchange interaction, two cation orbitals overlap the same *p* orbital of a shared anion in a cation-anion-cation bridge. The maximum spin transfer occurs when the angle of the cation-anion-cation bridge is ~180° and decreases when the angle diminish toward ~90°. The intensity of the superexchange interaction is highly dependent of that angle. Results from X-ray diffraction show that the angles RE1-O-RE2 and RE2-O-RE2 (RE1 = rare-earth element at the symmetric site; RE2=RE element at the asymmetric site) are in the range from ~99° to ~125° for both samples (see Table I) which indicates a weak superexchange interaction as revealed by the low B_{hf} measured for ^{111}Cd at asymmetric sites. The distance between two nearest neighbor rare-earth atoms (RE1-RE2 or RE2-RE2) is smaller for Er_2O_3 than for Gd_2O_3 (see Table II), which indicates that the intensity of B_{hf} measured with ^{111}Cd at the asymmetric sites must be higher for Er_2O_3 than for Gd_2O_3. This is because B_{hf} depends on the inverse of the cube of the distance between the probe and the magnetic atoms. PAC measurements have confirmed this prediction.

TABLE I. Angles between RE-O-RE. RE1=RE in the symmetric site and RE2=RE in the asymmetric site.

Gd1-O-Gd2 (degree)	Gd2-O-Gd2 (degree)	Er1-O-Er2 (degree)	Er2-O-Er2 (degree)
102.040(6)	100.181(4)	101.521(10)	100.015(6)
99.621(4)	124.325(3)	99.024(6)	125.522(5)
123.603(3)	101.495(6)	124.137(5)	100.291(11)

TABLE II. Distances between RE and the first neighbor, in Å. RE1=RE in the symmetric site and RE2=RE in the asymmetric site.

Gd1-Gd2	Gd2-Gd2	Er1-Er2	Er2-Er2
3.6054	3.6190(2)	3.4970(5)	3.5138(4)

V. CONCLUSIONS

PAC measurements were performed in Gd_2O_3 and Er_2O_3 NPs with and without the application of an external magnetic field of around 0.5 T. Results have shown that, when the probe is located at the symmetric site, the hyperfine magnetic field is close to zero, for both samples. On the other hand, when the probe occupies the asymmetric site, hyperfine magnetic fields of ~4 T and ~5 T are observed for Gd_2O_3 and Er_2O_3, respectively. From these PAC results, it was possible to determine that rare-earth atoms are coupled via a weak superexchange interactions. Finally, we have shown an interesting tool joining external fields plus local interactions as a way to obtain local magnetic properties in NPs.

ACKNOWLEDGMENTS

Authors acknowledge Wanderson Lobato for the bixbyite sites images. Financial support for this study was partially provided by the Conselho Nacional de Desenvolvimento Científico e Tecnológico (CNPq) [grant number 430060/2018-1] and Fundação de Amparo à Pesquisa do Estado de São Paulo (FAPESP) [grant number 2017/50332-0].

REFERENCES

[1] M. Tang, P. Lu, J. A. Valdez, and K. E. Sickafus, Journal of Applied Physics **99**, 063514 (2006).
[2] E. L. Correa, B. Bosch-Santos, F. H. M. Cavalcante, B. S. Correa, R. S. Freitas, A. W. Carbonari, and M. P. A. Potiens, AIP Advances **6**, 056112 (2016).
[3] E. L. Correa, B. Bosch-Santos, R. S. Freitas, M. P. A. Potiens, M. Saiki, and A. W. Carbonari, Nanotechnology **29**, 205704 (2018).
[4] M. N. Azlan, M. K. Halimah, R. El-Mallawany, M. F. Faznny, and C. Eevon, Journal of Materials Science: Materials in Electronics **28**, 4318 (2017).
[5] J. J. Ibarra-Sánchez, T. López-Luke, G. Ramírez-García, S. Sidhik, T. Córdova-Fraga, J. J. Bernal-Alvarado, M. E. Cano, A. Torres-Castro, and E. de la Rosa, Journal of Magnetism and Magnetic Materials **465**, 406 (2018).
[6] M. J. Alizadeh, H. Kariminezhad, A. S. Monfared, A. Mostafazadeh, H. Amani, F. Niksirat, and R. Pourbagher, Materials Research Express **6**, 065025 (2019).
[7] V. Narang, D. Korakakis, and M. S. Seehra, Journal of Magnetism and Magnetic Materials **368**, 353 (2014).
[8] E. Swatsitang, S. Phokha, S. Hunpratub, and S. Maensiri, Physica B: Condensed Matter **485**, 14 (2016).
[9] X. Wu, Z. Ding, N. Song, L. Li, and W. Wang, Ceramics International **42**, 4246 (2016).
[10] K. Elayakumar, A. Dinesh, A. Manikandan, M. Palanivelu, G. Kavitha, S. Prakash, R. T. Kumar, S. K. Jaganathan, and A. Baykal, Journal of Magnetism and Magnetic Materials **476**, 157 (2019).
[11] R. Hanada, CYRIC Annual Report, 1994.
[12] B. Bosch-Santos, A. W. Carbonari, G. A. Cabrera-Pasca, and R. N. Saxena, Journal of Applied Physics **115**, 17E124 (2014).
[13] M. Zacate and H. Jaeger, Defect and Diffusion Forum **311**, 3 (2011).

[14]V. S. Rudenko and A. G. Boganov, Inorganic Materials **6**, 1893 (1970).
[15]A. Saiki, N. Ishizawa, N. Mizutani, and M. Kato, Yogyo Kyokaishi **93**, 649 (1985).
[16]D. Lupascu, A. Bartos, K. P. Lieb, and M. Uhrmacher, Zeitschrift für Physik **93**, 441 (1994).
[17]B. Bosch-Santos, N. M. Nascimento, M. Saiki, E. L. Correa, T. S. N. Sales, L. F. D. Pereira, G. A. Cabrera-Pasca, R. N. Saxena, J. Schell, and A. W. Carbonari, AIP Advances **9**, 035245 (2019).
[18]F. H. M. Cavalcante, O. F. L. S. Leite Neto, H. Saitovitch, J. T. P. D. Cavalcante, A. W. Carbonari, R. N. Saxena, B. Bosch-Santos, L. F. D. Pereira, J. Mestnik-Filho, and M. Forker, Physical Review B **94**, 064417 (2016).
[19]J. Shitu, D. Wiarda, T. Wenzel, M. Uhrmacher, K. P. Lieb, S. Bedi, and A. Bartos, Physical Review B **46**, 7987 (1992).
[20]J. B. Goodenough, Journal of Physics and Chemistry of Solids **6**, 287 (1958).
[21]J. Kanamori, Journal of Physics and Chemistry of Solids **10**, 87 (1959).